

# On the light echo in V838 Mon

R. Tylanda

N. Copernicus Astronomical Center, Department for Astrophysics, Rabiańska 8, 87–100 Toruń, Poland

Received ; accepted

**Abstract.** After having presented a theoretical outline of the light echo phenomenon and results of simple numerical simulations we study the available images of the light echo in V838 Mon obtained with HST. From an analysis of the observed expansion of the light echo we conclude that the distance to V838 Mon is greater than  $\sim 5$  kpc. We also investigate the structure of the dust distribution in the vicinity of the object. We find no obvious signs of spherical symmetry in the resultant distribution. Near the central object there is a strongly asymmetric dust-free region which we interpret as an evidence that V838 Mon is moving relatively to the dusty medium. From these results we conclude that dust illuminated by the light echo is of interstellar origin rather than produced by mass loss from V838 Mon in the past.

**Key words.** stars: individual: V838 Mon – stars: distances – stars: circumstellar matter – ISM: reflection nebulae

## 1. Introduction

V838 Mon was discovered in eruption in the beginning of January 2002 (Brown 2002). The main outburst, however, started in the beginning of February 2002 and, in the optical, lasted for about two months (e.g. Munari et al. 2002a). The nature of the eruption is enigmatic (e.g. Munari et al. 2002a, Kimeswenger et al. 2002). It cannot be accounted for by known thermonuclear events (classical nova, late He-shell flash) so new, unexplored so far, mechanisms have been searched for (Soker & Tylanda 2003, Retter & Marom 2003).

V838 Mon has recently received significant publicity, even in non-scientific media, due to its light echo. This event has been discovered shortly after the main eruption in February 2002 (Henden et al. 2002). However, the most spectacular images of the V838 Mon light echo have been provided in later epochs by HST (Bond et al. 2003).

The light echo is a rare event and can be observed when a light outburst illuminates circumstellar or interstellar dust. So far it has primarily been observed for extragalactic supernovae (e.g. Chevalier 1986, Xu et al. 1995). In our Galaxy this phenomenon has been observed in Nova Persei 1901 (e.g. Couderc 1939).

Analyses of light echoes can be used while investigating supernova light curves (e.g. Chevalier 1986). Observed evolution of the light echo around SN 1987A in LMC has enabled to study the dust distribution in front of the supernova up to a distance of  $\sim 1$  kpc (see e.g. Xu et al.

1995). Supernova light echoes can also be used to measure distances to galaxies (Sparks 1994).

Munari et al. (2002a) and Kimeswenger et al. (2002) have attempted to use the observed expansion of the light echo around V838 Mon to measure the distance. Their calculations have however been based on a naive interpretation of the light echo expansion (i.e. that it expands at the velocity of light) and the derived values of 0.6–0.8 kpc are in fact significant underestimates of the distance. A more realistic analysis in Bond et al. (2003) gave a lower limit to the distance of  $\sim 6$  kpc.

In this paper we present an analysis of the available data on the light echo in V838 Mon. After presenting theoretical considerations and results of simple simulations of light echoes (Sect. 2) we attempt to use the observational data to constrain the distance to V838 Mon (Sect. 3) and to study the dust distribution in front of the object (Sect. 4).

## 2. Basic considerations and numerical simulations

Couderc (1939) was probably the first to give a correct explanation for the light echo arcs observed around Nova Persei 1901. More recently, theoretical considerations on the light echo can be found in papers devoted to supernova light echoes (see e.g. Chevalier 1986). The subject is however relatively unknown in the field of stellar astrophysics. This is probably the reason why in some papers oversimplified or even incorrect interpretations of the V838 Mon light echo can be found. Therefore let us summarize basic formulae describing the structure and evolution of the light echo.

---

Send offprint requests to: R. Tylanda, email: tylanda@ncac.torun.pl

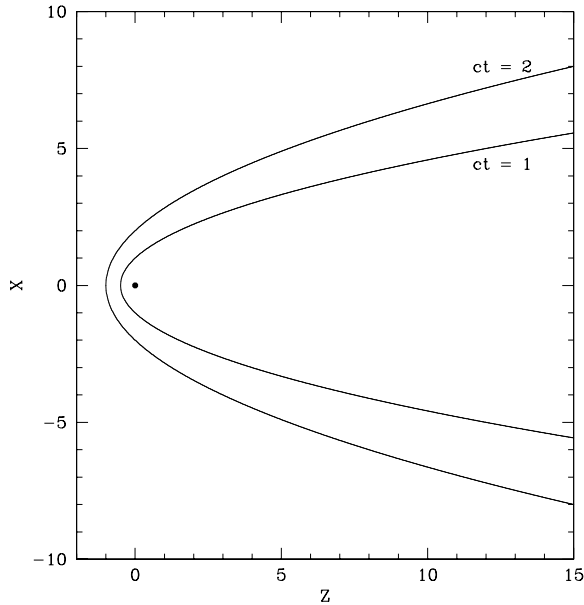


**Fig. 1.** The light echo paraboloid (Eq. 2) shown in the  $xz$  plane for  $ct = 1$  and  $ct = 2$ . The axes are in units of  $ct$ . The dot marks the source position at  $x = 0, z = 0$ . The observer is at  $x = 0, z = \infty$ .

Let us define a rectangular  $(x, y, z)$  coordinate system with its origin being in the light source. The  $z$  axis is along the line of sight toward the observer. The  $(x, y)$  plane is perpendicular to the  $z$  axis, i.e. is tangent to the sky sphere in the source. Let the source emit a short light flash at a time  $t = 0$ . We assume the so-called single scattering approximation, i.e. that photons are scattered only once in the dusty medium surrounding the source. Suppose that the scattered echo is seen by the observer at a time  $t$ . Then the illuminated dust lies on a surface defined by

$$r + l = d + ct \quad (1)$$

where  $c$  is the velocity of light,  $d$  is the distance between the source and the observer,  $r = \sqrt{x^2 + y^2 + z^2}$  is the distance of the scattering dust from the source, and  $l = \sqrt{x^2 + y^2 + (d - z)^2}$  is the distance of the dust from the observer. Eq. (1) is an ellipsoid having foci in the source and the observer.

The considerations can be simplified when  $x$  and  $y$  are much smaller than  $d$ , i.e. when the observed angular dimensions of the echo are small. Putting  $l = d - z$  Eq. (1) becomes

$$x^2 + y^2 = (ct)^2 + 2zct. \quad (2)$$

This is a paraboloid symmetric around the  $z$  axis (line of sight) and having focus in the source. In the case of V838 Mon the echo has dimensions of order of  $1'$  so in this case the accuracy of Eq. (2) is better than  $10^{-3}$ .

Figure 1 shows Eq. (2) in the  $xz$  plane for  $ct = 1$  and  $ct = 2$  (axes in the figure are in units of  $ct$ ). Several important conclusions can be drawn from Fig. 1. If the source

(at  $x = 0, z = 0$ ) has produced a short flash of light at  $t = 0$  then at  $t = 1/c$  and  $t = 2/c$  the observer would see dust illuminated on paraboloids  $ct = 1$  and  $ct = 2$ , respectively. However, if the flash started at  $t = 0$  and lasted up to  $t = 1/c$  then at  $t = 1/c$  all dust within the paraboloid  $ct = 1$  would be illuminated for the observer. At  $t = 2/c$  illuminated dust would be between the paraboloids  $ct = 1$  and  $ct = 2$ . Thus contrary to some naive considerations the echo does not expand spherically starting from the source. It starts from the line of sight, i.e.  $x = 0, z \geq 0$ , and most effectively penetrates regions situated in front of the source. Behind the source the penetration is slowest.

The observed echo is in the  $(x, y)$  plane and its structure and evolution depends on the dust distribution around the source. One of important conclusions which can easily be drawn from Fig. 1 is that if the observed echo has a well defined outer rim (as observed in the case of V838 Mon) the dusty medium around the source has to have a rather well defined outer boundary in front of the source.

In order to illustrate dependence of the light echo structure and evolution on the dust distribution let us consider two simple dust geometries, i.e. a plane parallel slab and a spherical shell centred on the source.

### 2.1. Plane parallel dust slab

Let us assume that a thin plane parallel slab of dust intersects the line of sight at  $z_0$  and that the normal to the slab is inclined to the  $z$  axis at an angle  $\alpha$ . Let us also assume, for simplicity, that the normal lies in the  $(x, z)$  plane. The slab is then described by

$$z = z_0 - ax \quad (3)$$

where  $a = \tan \alpha$ . Eq. (3), when used to eliminate  $z$  from Eq. (2), gives the echo shape as follows

$$x^2 + y^2 = (ct)^2 + 2z_0ct - 2axct. \quad (4)$$

Thus the echo is in the shape of a ring whose radius,  $r_e$ , is given by

$$r_e = \sqrt{(1 + a^2)(ct)^2 + 2z_0ct}. \quad (5)$$

The ring is centred at

$$x_c = -act, y_c = 0. \quad (6)$$

The velocity of expansion of the echo ring,  $v_e$ , is

$$v_e \equiv \frac{dr_e}{dt} = \frac{(1 + a^2)c^2t + z_0c}{r_e} = \frac{(1 + a^2)c^2t + z_0c}{\sqrt{(1 + a^2)(ct)^2 + 2z_0ct}}. \quad (7)$$

An analysis of Eqs. (5 – 7) leads to the following conclusions. The echo ring is centred on the source only if the dust slab is perpendicular to the line of sight. In almost all the cases the echo expansion is superluminal. Only if  $z_0 = 0$  and  $a = 0$  the echo expands at  $c$ . For  $z_0 > 0$  (the slab in front of the source) the echo appears at the same time as the source flash, i.e. at  $t = 0$ . It starts expanding

from the source position, i.e. from  $x_c = 0, y_c = 0$ . For  $z_0 < 0$  (the slab behind the source) the echo appears with a time delay relative to the source flash, i.e. it starts at  $t = (-2z_0)/((1 + a^2)c)$ . In this case it begins expanding from the position  $x_c = (2z_0a)/(1 + a^2), y_c = 0$ . In both cases the expansion velocity is  $\infty$  at the moment of the echo appearance, i.e. at  $t = 0$  if  $z_0 > 0$  and at  $t = (-2z_0)/((1 + a^2)c)$  if  $z_0 < 0$ . It decreases asymptotically to  $\sqrt{1 + a^2}c$  when  $(1 + a^2)ct \gg |z_0|$ . For slabs non-perpendicular to the line of sight, i.e. when  $a \neq 0$ , the echo centre moves away from the source at a constant velocity of  $|a|c$ . The direction of this movement is opposite to the direction of the slab normal projected on the sky surface.

## 2.2. Spherical dust shell

Let us assume that a thin spherically symmetric shell of dust having a radius,  $r_0$ , is centred on the source, so it is described by

$$r_0^2 = x^2 + y^2 + z^2. \quad (8)$$

This when used to eliminate  $z$  from Eq. (2) gives

$$x^2 + y^2 = 2r_0ct - (ct)^2. \quad (9)$$

Thus the echo is in the shape of a ring with the radius,  $r_e$ , given by

$$r_e = \sqrt{2r_0ct - (ct)^2} \quad (10)$$

and centred on the source ( $x_c = 0, y_c = 0$ ). The echo expansion velocity,  $v_e$ , is

$$v_e \equiv \frac{dr_e}{dt} = \frac{r_0c - c^2t}{r_e} = \frac{r_0c - c^2t}{\sqrt{2r_0ct - (ct)^2}}. \quad (11)$$

As can be seen from Eq. (10), the echo radius starts from zero at  $t = 0$ , reaches a maximum equal to  $r_0$  at  $t = r_0/c$ , and collapses to zero at  $t = 2r_0/c$ . Note that in a coordinate system  $(ct - r_0, r_e)$  Eq. (10) describes a circle centred on the origin and having the radius equal to  $r_0$ . The expansion velocity of the echo ring starts from  $\infty$  at  $t = 0$ , decreases and reaches zero at  $t = r_0/c$ , and continues decreasing to  $-\infty$  at  $t = 2r_0/c$ .

## 2.3. Numerical simulations

In order to illustrate the evolution of the echo in different geometries of the dust distribution we have performed simple numerical simulations based on the theoretical considerations outlined above. The structure of the light echo has been determined in the paraboloid approximation, i.e. using Eq. (2). If the central source radiates at a luminosity,  $L_\nu$ , the intensity,  $I_\nu$ , of the radiation scattered at a point  $(x, y, z)$  after the time delay,  $t = r/c$  (where  $r = \sqrt{x^2 + y^2 + z^2}$ ), can be calculated from

$$I_\nu = \frac{\sigma_\nu L_\nu}{16\pi^2 r^2}. \quad (12)$$

Here  $\sigma_\nu$  is the scattering coefficient. Eq. (12) adopts the single scattering approximation and that the scattering is isotropic. Integrating Eq. (12) along the  $z$  axis over the dusty medium illuminated at a given time,  $t$ , gives the echo surface brightness at the point  $(x, y)$  at this time moment.

The simulations have been done for two simple geometries of the dust distribution, similarly as above. In the case presented in Fig. 2 dust has been adopted to be uniformly (i.e. having constant  $\sigma_\nu$ ) distributed in four plane parallel slabs perpendicular to the  $z$  axis. The  $z_0$  positions of the slabs are  $-0.10, 0.00, 0.30$ , and  $1.00$  pc. The slab thickness is the same in all cases and is equal to  $0.02$  pc.  $L_\nu$  has been adopted to be constant during the source flash which lasted for 50 days (otherwise  $L_\nu = 0$ ). Fig. 2 shows the echo structure as observed from a distance of 5 kpc at 50, 150, 250, 300, 400, and 500 days after the beginning of the flash. The grey scale is logarithmic and it has been normalized to the maximum surface brightness in the images. Between the brightest centre of the first image and the faintest outer ring in the last image there is a span of 4 orders of magnitude in the surface brightness.

The first image in Fig. 2 shows the echo just at the end of the source flash. According to the discussion of Fig. 1 all dust being within the paraboloid defined by the time elapsed since the beginning of the flash, is illuminated. Thus the echo is composed of three filled circles produced by three slabs having  $z_0 \geq 0.0$  (the fourth slab at  $z_0 = -0.1$  pc is not seen as it has not yet been reached by the light paraboloid). Later on the illuminated dust is situated between two paraboloids, i.e. the first one corresponding to the beginning of the flash and the second one defined by the epoch of the end of the flash. Thus in the second image, taken 100 days after the end of the flash, the echo consists of three rings. The slab at  $z_0 = -0.10$  pc is reached by the first paraboloid at  $t \simeq 210$  days, whereas the second paraboloid starts leaving it at  $t \simeq 310$  days. Therefore this slab is seen in the form of a central disc in the third and fourth image. Later on it produces the innermost ring in the image.

As can be seen from Fig. 2 the surface brightness of the rings decreases with time. For geometrical reasons the decrease is strongest for the slab at  $z_0 = 0.0$ . From the first image to the last one in Fig. 2 the surface brightness in the ring corresponding to  $z_0 = 0.0$  decreases by factor  $\sim 500$  whereas the same drop in the case of the outermost ring ( $z_0 = 1.00$  pc) is only factor  $\sim 2$ . With time the echo rings would continue expanding with slowly decreasing surface brightness and with the expansion velocity approaching  $c$ .

Figure 3 shows the evolution of the echo structure produced by three spherically symmetric dust shells centred on the source. The radii of the shells are  $0.10, 0.30$ , and  $1.00$  pc. All the shells have the same thickness equal to  $0.02$  pc. As in the previous case the source flash has lasted for 50 days and the object is observed from a distance of 5 kpc. The consecutive images correspond to the epochs of 50, 150, 250, 400, 600, and 750 days after the beginning of the source flash.

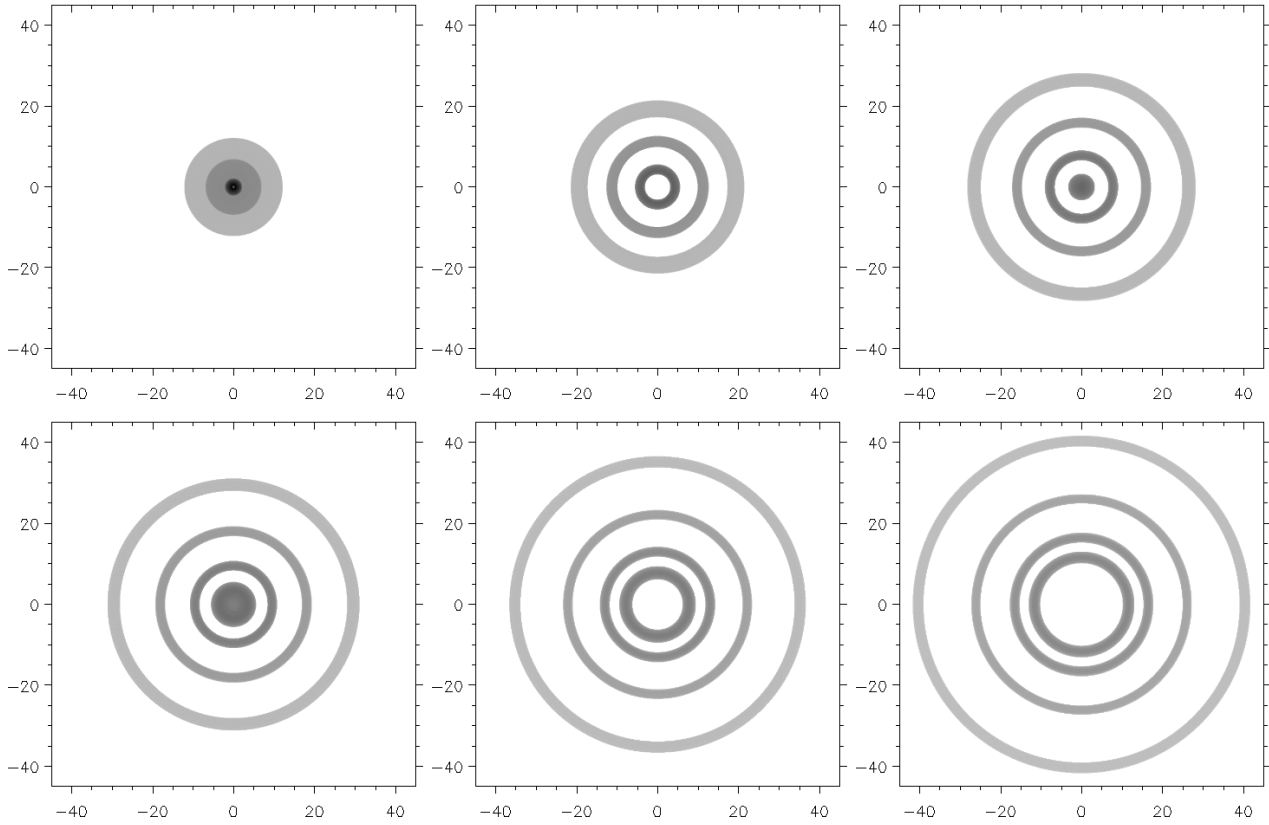


**Fig. 2.** The evolution of the echo structure produced by four dust slabs perpendicular to the line of sight at the  $z$  positions of  $-0.10$ ,  $0.00$ ,  $0.30$ , and  $1.00$  pc. The source (not shown in the figure but lying in the centre of each image) has experienced a 50 days long flash of constant luminosity. All the slabs have the same thickness of  $0.02$  pc and the same value (constant within the slabs) of the scattering coefficient  $\sigma_\nu$ . The object is assumed to be observed from a distance of 5 kpc. The images are ordered from upper-left to lower-right and correspond to the time epochs of 50, 150, 250, 300, 400, and 500 days after the beginning of the source flash. The axes of the images are in arcsec. The grey scale is logarithmic and is normalized to the brightest region in the figure. The brightest centre of the first image and the faintest outer ring in the last images span  $\sim 4$  orders of magnitude in the surface brightness.

As in Fig. 2 the first image in Fig. 3 corresponds to the end of the source flash and all dust within the light paraboloid produced by the beginning of the flash is illuminated. The echo is thus composed of three filled circles produced by illuminated sections of the corresponding shells. The echo components initially expand superluminally. However, as discussed in Sect. (2.2), the echo from a shell slows the expansion rate down to 0 when reaching the maximum radius equal to the value of  $r_0$ . For the shells in our simulations, i.e. having  $r_0 = 0.1$ ,  $0.3$ , and  $1.0$  pc, it happens at  $t \simeq 130$ ,  $370$ , and  $1200$  days, respectively. At the same time the echo ring gets its maximum surface brightness and minimum thickness. Next the echo ring starts shrinking and finally disappears as a fast collapsing disc. In our simulations the echoes due to the shells having  $r_0 = 0.1$ ,  $0.3$ , and  $1.0$  pc disappear at  $t = 310$ ,  $790$ , and  $2450$  days. In the second image in Fig. 3 the innermost ring is close to its maximum radius whereas in the third image the echo from the innermost shell is collapsing. The echo from the shell having  $r_0 = 0.3$  pc is close to its maximum radius in the fourth image whereas its collapse is observed in the last two images.

#### 2.4. Discussion

The above considerations, although done for simplified cases, demonstrate that long term observations of the evolution of the echo structure can provide information on the dust distribution and thus, indirectly, also on the origin of the dust producing the echo. If dust results from a past mass loss from the central object it would tend to show certain symmetries in its distribution around the source. Usually mass loss is not continuous at a constant rate but rather in form of more or less periodic fluctuations of the mass loss rate, e.g. during the AGB phase, or discrete events of strong mass loss separated by longer periods of quiescence, e.g. in nova-like outbursts. Then the dust distribution would show a succession of shell-like structures or be in form of a more or less defined envelope. The evolution of the light echo in such circumstances would follow general patterns discussed in Sect. 2.2 and Fig. 3. The initially fast expansion, slowing down when reaching maximum sizes corresponding to outer edges of the dust shells or envelope would be followed by an accelerated collapse.

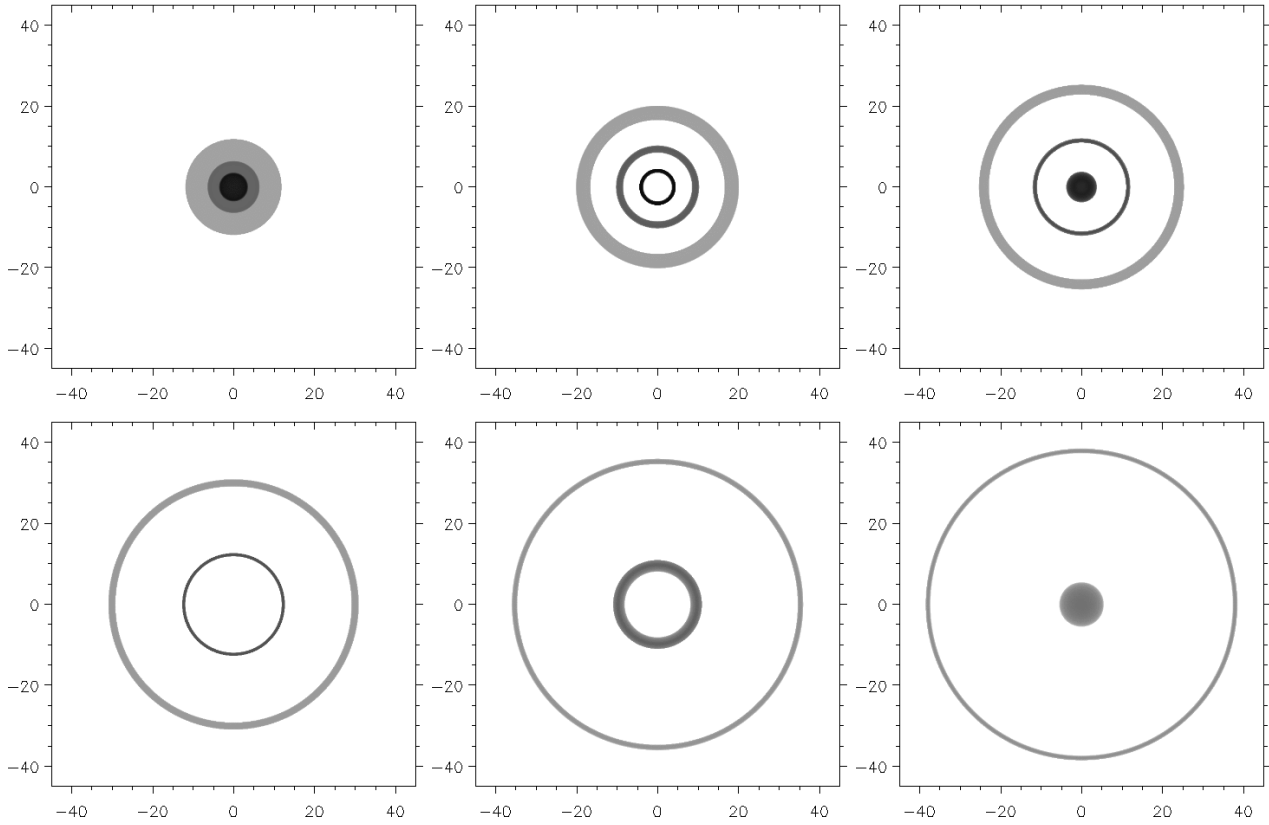


**Fig. 3.** The same as Fig. 2 but for three spherical shells of dust centred on the source. The shells have the same thickness of 0.02 pc and radii of 0.10, 0.30, and 1.00 pc. The images show the echo as observed 50, 150, 250, 400, 600, and 750 days after the beginning of the source flash. The brightest and the faintest regions in the figure span  $\sim 2.5$  orders of magnitude in the surface brightness.

If, however, dust is not related to the source and is rather of interstellar character no obvious symmetry in respect to the light source is expected to occur in its distribution. Instead dust would rather be in form of extended sheets, zones or filaments and our considerations of plane parallel slab geometries in Sect. 2.1 and Fig. 2 would be more appropriate. The echo would expand more and more with slowly decreasing brightness as more and more distant regions are illuminated.

Note that for studying the general character of the dust distribution around the source the echo has to be observed for a long enough time. The initial evolution of the echo produced by spherical dust shells is similar to that due to slabs. The light paraboloid is close to the line of sight so the echo does not feel differences in the general shape of the dust distribution. This can be seen from Eqs. (5) and (10) which reduce to the same form if  $ct \ll z_0$  and  $ct \ll r_0$ , respectively. Thus the first image in Fig. 3 is not much different from that in Fig. 2 (the reason why the innermost (brightest) disc in Fig. 2 is significantly smaller than the corresponding one in Fig. 3 is that in the former case it is produced by the slab at  $z_0 = 0.0$  whereas in the latter case the shell has  $r_0 = 0.1$  pc). Later on, when  $ct$  is no more negligible compared to  $z_0$  and  $r_0$  the differences between the geometries are better and better seen in the echo evolution.

### 3. Distance to V838 Mon constrained from the echo expansion

An analysis of the light echo evolution can be used to estimate the distance to the object. One possible way of doing that using the observed polarization structure of the echo has been proposed in Sparks (1994). An attempt to derive the distance to V838 Mon has been done in Bond et al. (2003). They measured expansion rates of ring-like structures in the echo from two consecutive images and found that the distance is greater than 2 kpc. An attempt to use the method proposed by Sparks (1994) led Bond et al. to conclude that the lower limit to the distance is  $\sim 6$  kpc.

We have attempted to put constraints on the distance to V838 Mon from measuring expansion of the outer edge of the echo. As it is clear from the considerations in Sect. 2 the outer edge of the echo is produced by the beginning of the light flash reflected at the outermost edge of the dust distribution in front of the source.

For the plane slab geometry Eq. (5) when combined with Eq. (6) can be rewritten as

$$\theta = \frac{r_e}{d} = \sqrt{\left(\frac{2z_0}{ct} + 1\right)\left(\frac{ct}{d}\right)^2 + \theta_c^2} \quad (13)$$

**Table 1.** Results of fitting a circle to the outer edge of the light echo of V838 Mon. Time is in days since 1 January 2002. Results are in arcsec.

$t(\text{days})$	$\theta$	$\epsilon$	$x(\text{centre})$	$y(\text{centre})$
120.0	18.55	1.08	-0.84	0.46
140.0	20.89	1.05	-1.12	0.51
245.0	30.32	1.44	-2.27	0.37
301.0	33.68	1.46	-2.36	1.11
351.0	36.66	1.56	-2.61	1.58

where  $d$  is the distance to the object,  $\theta$  is the angular radius of the echo, and  $\theta_c = x_c/d$  is the angular distance of the echo centre from the source. At early epochs, i.e. when  $(2z_0)/(ct) \gg 1$ , Eq. (13) allows to determine only the value of  $z_0/d^2$ . Thus unless  $z_0$  is known the distance cannot be determined. However, in later epochs, when  $(2z_0)/(ct) \ll 1$ , Eq. (13) can be used to derive  $d$  from the observed values of  $\theta$  and  $\theta_c$ .

In the case of the spherical symmetry Eq. (10) can be rewritten as

$$\theta = \sqrt{\left(\frac{2r_0}{ct} - 1\right)\left(\frac{ct}{d}\right)^2}. \quad (14)$$

Thus, not only in early phases (fast initial expansion) but also in late phases (final collapse) the distance cannot be determined unless the value of  $r_0$  is known. Only near the maximum size of the echo, i.e. when  $r_0 \approx ct$ , Eq. (14) can give a direct estimate of the distance.

In a real case, such as V838 Mon, we do not know a priori what is the distance of the outer edge of dust from the source nor what is the geometry of this edge. Thus the only way is to look at the observed evolution of the echo and try to fit it with Eq. (13) or Eq. (14).

For this purpose we have measured the positions of the outer edge of the light echo of V838 Mon on five images taken by H.E. Bond and available at the HST web site (<http://hubblesite.org/newscenter/archive/2003/10/>, see also Bond et al. 2003). The images cover the period from April 30 to December 17, 2002. From each image the positions of typically 60–70 points at the outer rim of the echo (more or less equally spaced in the azimuthal angle) have been measured. Note that all the measurements (also those reported in the next section) have been done on the negatives of the published images as then corresponding emission edges are more easily seen. The positions have been determined in the coordinate system centred on V838 Mon with the  $x$  and  $y$  axes pointing to west and north, respectively. Then a circle has been fitted to the measured positions on each image using the least square method. The results are presented in Table 1. First column shows the time of observations given in days since January 1, 2002. The radius of the echo,  $\theta$ , and its uncertainty,  $\epsilon$ , (measured as a standard deviation of the observed points from the fitted circle) are given in the next two columns. The last two columns show the position of the centre of the fitted circle relative to the central star. All the results are in arcsec.

In order to make a quantitative analysis of the results in Table 1 it is necessary to determine the time moment of the zero age of the echo,  $t_0$ . The echo has been discovered in mid-February 2002 (Henden et al. 2002) and it has been suggested that the observed echo results from the main outburst which started in the beginning of February 2002 (Munari et al. 2002a, Bond et al. 2003). This is supported by the fact that in the HST images the outer echo rim is blue and it was in the beginning of the main outburst when the star was bluest (see e.g. Bond et al. 2003). The main outburst started on February 1 and the maximum has been reached on February 5–6 (Munari et al. 2002a, Bond et al. 2003). Thus we adopt February 3 as the date of the zero age of the echo, i.e.  $t_0 = 34$  days.

As can be seen from Table 1, the centre of the echo migrates from the central star. The migration keeps more or less the same direction and the distance between the echo centre and the star increases roughly linearly with time since the zero age. This is what is expected from the plane geometry of the dust distribution (see Eq. 6). It cannot be reconciled with a spherically symmetric distribution. Thus the shape of the outer edge of dust in front of the star can be approximated by a plane inclined to the line of sight rather than a sphere centred on the star.

A linear fit to the observed evolution of the distance of the echo centre from the star as given in Table 1 results in a relation

$$\theta_c = (0'.0106 \pm 0'.0008)\left(\frac{t}{1 \text{ day}}\right) \quad (15)$$

where  $t$  is the time since the zero age of the echo. This with Eq. (6) allows to derive the inclination of the dust surface to the line of sight, i.e.

$$\tan \alpha = (0.061 \pm 0.005)\left(\frac{d}{1 \text{ kpc}}\right). \quad (16)$$

Unfortunately the distance cannot be determined with a satisfactory accuracy (see below). Adopting  $d = 5$  kpc one obtains  $\alpha \simeq 16^\circ$  whereas for  $d = 10$  kpc Eq. (16) gives  $\alpha \simeq 30^\circ$ . Note that the azimuthal angle of the normal to the dust surface is opposite (i.e.  $+180^\circ$ ) to that of the echo centre.

A  $\chi^2$  minimum fit of Eq. (13) to the observed values of  $\theta$  in Table 1 gives the best fit for  $d \simeq 6.1$  kpc and  $z_0 \simeq 2.0$  pc. However the  $\chi^2$  minimum is rather shallow and extended along a  $z_0 \sim d^2$  relation. From a 90% confidence level on the  $(d, z_0)$  plane we can only state that the lower limit to the distance is  $\sim 2.5$  kpc.

Clearly we are well before the phase when the distance can be unambiguously determined, i.e. when  $(2z_0)/(ct) \ll 1$ . Another reason for the large uncertainty in the distance estimate is in significant uncertainties in the observed values of the echo radius in Table 1. These uncertainties are simply due to the fact that the echo rim is not ideally reproduced by a circle. Clearly the outer edge of the dust distribution in front of V838 Mon is not a perfect plane.

We have, however, found that in the north-west quadrant, i.e. for  $x > 0$  and  $y > 0$ , the echo rim is well defined

**Table 2.** Results of fitting a circle centred on the star to the north-west quadrant ( $x > 0, y > 0$ ) of the outer edge of the light echo of V838 Mon. Time is in days since 1 January 2002. Results are in arcsec.

$t(\text{days})$	$\theta$	$\epsilon$
120.0	18.46	0.32
140.0	20.59	0.19
245.0	28.83	0.36
301.0	32.83	0.44
351.0	36.02	0.45

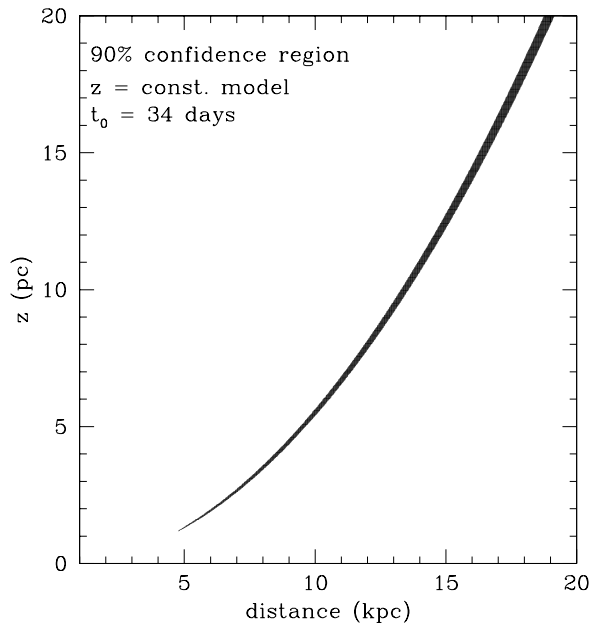


**Fig. 4.** The 90% confidence region of the  $\chi^2$  test of fitting Eq. (13) to the data in Table 2.

and its shape can be quite well reproduced by a circle centred on the star. The results of a least square fit of a circle centred on the star to the observed echo rim in the north-west quadrant are given in Table 2. As can be seen from Table 2 the fit is here significantly better (lower  $\epsilon$ ) than that in Table 1.

A  $\chi^2$  minimum fit of Eq. (13) to the data in Table 2 gives the best fit for  $d \simeq 9.0$  kpc and  $z_0 \simeq 4.5$  pc. The 90% confidence region from this fit is shown in Fig 4. Although the 90% confidence region is more confined than in the previous case but still the uncertainty in the distance is large. All what can be said is that the distance to V838 Mon is greater than  $\sim 4.8$  kpc.

The echo in the shape of a circle centred on the source can also be modelled by a spherically symmetric distribution of dust. Therefore we have also attempted to fit Eq. (14) to the data in Table 2. The  $\chi^2$  test has however been unable to find a minimum. It gives acceptable fits starting from  $d \simeq 7$  kpc but finds better and better fits for the distance increasing and increasing, well beyond reasonable limits. Clearly the test "prefers" the situation in which a sphere section illuminated by the echo is closer

and closer to a plane. This suggests that the constant  $z$  model better approximates the outer edge of dust in the north-west quadrant of the V838 Mon echo than the spherical model.

#### 4. Structure of the dust region in front of V838 Mon

The structure of the light echo observed in V838 Mon is rather complex especially in the last three images. This obviously reflects the complex distribution of the circumstellar dust. We have attempted to study this distribution from an analysis of the available images. Of course only dust illuminated by the light echo can be studied which practically limits the analysis only to the regions lying in front of V838 Mon.

In the available echo images, apart from the outer edge, one can also distinguish edges of the emission inside the echo. These edges are usually in colour either blue or red. From the light curve of V838 Mon it is clear that the object was bluest in the beginning of the outburst (beginning of February 2002) while during the fading (mid-April 2002) it was extremely red (Munari et al. 2002a, Bond et al. 2003). Suppose that the paraboloids  $ct = 2$  and  $ct = 1$  in Fig. 1 correspond to the blue beginning and the red end of the light flash, respectively. Suppose also that, say, between  $z = 5$  and  $z = 10$  there is a dust layer. Then the observer would see an echo ring whose outer edge would be blue and would correspond to the intersection of  $z = 10$  with  $ct = 2$ , while the inner edge would be red and would correspond to the intersection of  $z = 5$  with  $ct = 1$ . Thus measurements of the positions of the blue and red edges in the light echo of V838 Mon can be used to estimate positions of the boundaries of dust layers producing bright regions in the echo.

We have measured, apart from the outer edge discussed in Sect. 3, positions of blue and red edges inside the echo images. This concerns primarily the images taken on Sept. 2, Oct. 28 and Dec. 17 showing several well defined details in the echo structure. We have measured only the most obvious features which can be easily identified in all the three images. On the image from May 20 only the inner red edge has been measured (apart from the outer blue edge). On Apr. 30 only a B image has been taken so no red edge can be identified. Following the above considerations we adopt that the blue edges are produced by the beginning of the outburst so, as discussed in Sect. 3, they correspond to the light paraboloid with  $t_0 = 34$  days. From the I curve in Bond et al. (2003) it can be found that near Apr. 17 V838 Mon declined by factor 2 from its last peak. Therefore we adopt that the red edges in the light echo correspond to the paraboloid with  $t_0 = 107$  days.

Knowing  $x$  and  $y$  from measurements of an edge in the echo observed at a given time,  $t$ , one can calculate the  $z$  coordinate of the dust edge from Eq. (2). Obviously we measure only the angular values of  $x$  and  $y$  so in order to have their absolute values we have to adopt the distance. Unfortunately, as discussed in the previous section,

we have only been able to put the lower limit to the distance at  $\sim 5$  kpc. Munari et al.(2002b) have estimated  $d \simeq 10$  kpc from the magnitude of the B3V companion to V838 Mon. However, uncertainty of this estimate is probably significant. One of the reasons are uncertainties in calibrations of the absolute magnitudes of the BV stars (e.g. Wegner 2000). For the purpose of this section we have adopted that V838 Mon is at a distance of 8 kpc.

The results on the dust structure are presented in Fig. 5. It shows three cuts across the three dimensional distribution of the dust boundaries inferred from the measurements of the blue (open points) and red (full points) edges in the light echo. The plane of each part of Fig. 5 goes through the  $z$  axis and is inclined to the  $x$  (east-west) axis at an angle,  $\beta$ , (counted clockwise from the  $x$  axis) given in the bottom-left corner of each part of the figure. Only the points having the position angle within  $\beta \pm 15^\circ$  are shown. The axes are in unites of the mean  $z$  distance of all the points corresponding to the outer edge of the light echo. This mean  $z$  distance is 3.67 pc. Thin curves show the echo blue paraboloids (with  $t_0 = 34$  days) on Apr. 30 and Dec. 17. Thus, in principle, we can study only the dust distribution between these two paraboloids. Exception is the inner red edge on May 20 whose (red) paraboloid lies within the (blue) paraboloid on Apr. 30. Dust is present above full and below open symbols (it is absent above open and below full points).

The cuts shown in Fig. 5 have been chosen so as to show the global distribution of dust. They are more or less equally spaced in the azimuthal angle  $\beta$  but they also avoid too detailed structures which would make discussion too complicated and less clear. The author recommends consulting the original echo images (e.g. at <http://hubblesite.org/newscenter/archive/2003/10/>) for an easier understanding of the discussion below.

Fig. 5a shows the cut done close to ( $5^\circ$  inclined to the west from) the south-north direction. It goes more or less across the major axis of the central hole in the echo images. The dust distribution in this cut is very simple. In the southern part ( $x' < 0$  in Fig. 5a) dust extends from the hole boundary which lies very close to ( $\sim 0.2$  pc from) the central object up to  $\sim 3$  pc in  $z$ . In the northern part ( $x' > 0$ ) the empty region extends up to  $\sim 1.5$  pc. Then the dust region goes up to  $\sim 3.5$  pc.

The section in Fig. 5b goes close to ( $10^\circ$  inclined to the north from) the east-west direction. In the eastern part ( $x' < 0$ ) the central hole is rather compact (similarly as for  $x' < 0$  in Fig. 5a). Dust however extends only up to  $\sim 1.5$  pc. Then above there is an empty region. Only at  $\sim 4$  pc there is a thin dust layer. On the western side of the section ( $x' > 0$ ) the central hole extends up to  $\sim 1.5$  pc but more or less in the middle it is cut by a thin layer (or filament) of dust. Then a thick dust layer extends between  $\sim 1.5$  and  $\sim 3.5$  pc.

The last section presented in Fig. 5c have been done along the north-east – south-west direction. In the north-eastern part ( $x' < 0$ ) the dust structure is rather complex. A rather empty region extends from the central star up to

$\sim 1.0$  pc, although roughly in the middle there is a dusty region. The main dust region extends between  $\sim 1.0$  and  $\sim 2.5$  pc. Note however that this region has its own complex structure as can be best inferred from the echo image taken on Dec. 17. Finally at a distance of  $\sim 3.7$  pc there is a thin dust layer. In the south-western part an extended dust regions begins at  $\sim 0.2$  pc from the star and goes up to  $\sim 3.3$  pc.

The general picture that emerges from our analysis is as follows. Near the central object there is a strongly asymmetric region free of dust. Its boundary is relatively close to the star, i.e. at  $\sim 0.2$  pc, in the south-east, south and south-west directions. In the northern direction this hole extends up to  $\sim 1.5$  pc. In the north-east and north-west direction the situation is less clear. The empty region certainly extends to  $\sim 0.5$  pc. Further away there are some dusty regions but rather thin so one may argue that the central hole extends up to  $\sim 1.0$ – $1.5$  pc. Above the central hole there is the main dust region whose outer boundary in the north, west and south directions lies at  $\sim 3.0$ – $3.5$  pc. In all the eastern directions the boundary is closer to the star and near the east axis it is as close as  $\sim 1.5$  pc. Finally in the eastern directions there is a thin dust layer at a distance of  $\sim 4$  pc.

It should be finally reminded that all the absolute positions of the dust regions given above have been obtained adopting the 8 kpc distance to V838 Mon. The most sensitive to the value of distance is the  $z$  coordinate which depends on the square of the distance. Fortunately the relative picture of the dust distribution presented in Fig. 5 would be hardly affected if other values of the distance have been adopted.

In Sect. 3 while constraining the distance to V838 Mon we have approximated the outer rim of the observed echo in the north-west quadrant by a circle centered on the central star and interpreted the results as produced by a flat surface perpendicular to the line of sight. From the results in the present section it comes out that it was a reasonable assumption. The  $z$  values of the outer rim points from this quadrant (i.e. having  $x > 0$ ,  $y > 0$ ) are scattered around its mean value by less than 3% (standard deviation).

## 5. Conclusions and discussion

For all astrophysical objects it is important to know their distances. In the case of V838 Mon it is particularly important. The outburst of V838 Mon does not fit to any known class of outbursting stars so determination of its luminosity is crucial for attempts to identify the mechanism of the event. The early estimates of 0.6–0.8 kpc based on a naive interpretation of the light echo expansion (Munari et al. 2002a, Kimeswenger et al. 2002) led to the maximum luminosity of  $\sim 10^4 L_\odot$  which is typical for nova or nova-like outbursts. Our analysis presented in Sect. 3 clearly shows that the distance and thus also the luminosity are much greater. Unfortunately the presently available data on the echo evolution do not allow to determine the distance with



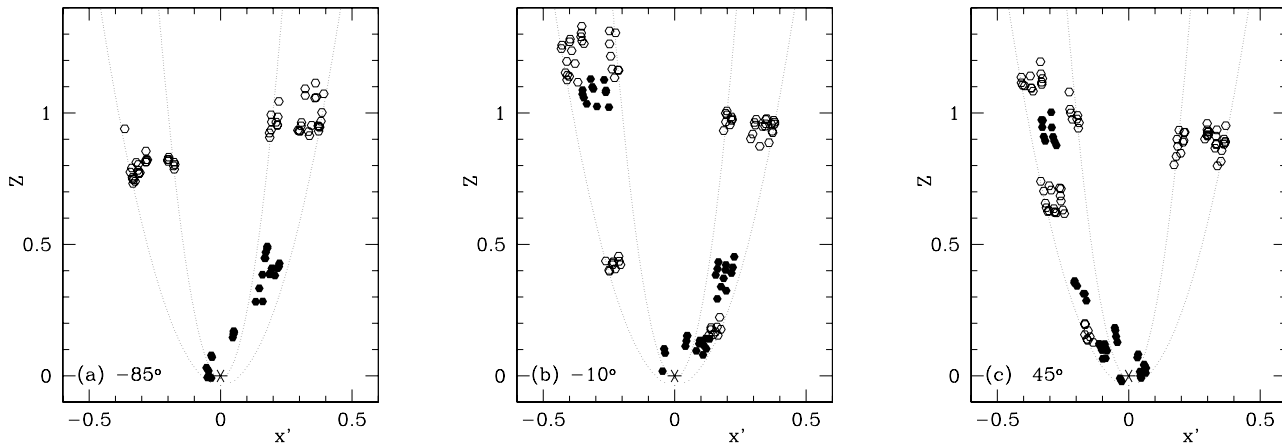


**Fig. 5.** Structure of the dust distribution illuminated by the light echo of V838 Mon. In all the images the ordinate is the  $z$  axis. The abscissa,  $x'$ , is inclined to the  $x$  (east-west) axis at an angle,  $\beta$ , (clockwise in respect to the  $x$  axis) given in the bottom-left corner of each image. Only the points having the position angle within  $\beta \pm 15^\circ$  are shown in each image. Open and full symbols correspond to upper and lower (in the  $z$  coordinate) boundaries of the dusty regions, respectively. Thin curves show the echo paraboloids (with  $t_0 = 34$  days) on Apr. 30 and Dec. 17. The axes are in units of the mean  $z$  distance of all the points in the outer edge of the light echo, which is 3.67 pc. The position of the central star is shown by an asterisk.

a satisfactory precision. But even our lower limit of  $\sim 5$  kpc makes the maximum luminosity  $\gtrsim 10^6 L_\odot$  which puts the outburst of V838 Mon to the most luminous events in our Galaxy. Unfortunately it seems that we will have to wait long time in order to obtain a reasonable estimate of the distance from the echo expansion. As discussed in Sect. 3 the condition for this is  $ct > z_0$ . If  $z_0 \simeq 3$  pc  $t$  should be at least 10 years.

As has been shown in Sect. 4 the evolution of the light echo can be used as a very useful tool for studying the dust distribution near the light source. Although the absolute characteristics of the obtained distribution depend on the distance, which is uncertain in the case of V838 Mon, the relative structure is fairly insensitive to this parameter. What we have done it is a rather simple analysis. A much more detailed study could be done on absolutely calibrated images of the echo which were not available to the author. Certainly further observations would be very valuable. When the light paraboloid becomes larger and larger, newer and newer regions of dust are illuminated and more and more complete image of the dust distribution in the vicinity of the star can be obtained. As can be seen from Fig. 5 only a small part of the volume around V838 Mon could have been studied so far. But even from it interesting conclusions can be made.

We have found no signs of spherical symmetry in the dust distribution which would have been expected if the observed dust had resulted from mass loss activities of V838 Mon in the past. The main dust regions has the outer boundary which is relatively flat and almost perpendicular to the line of sight in the western part. But near the south-north line it bends toward the central star or rather splits into a thin outer layer and a thicker zone closer to the central star. Near the central object there is a dust free region. This central hole is strongly asymmetric. Its boundary is quite close to the star in the southern

directions but in the northern directions it is at least 10 times further away (the boundary of the hole in north seems to be still outside the light paraboloid). The holes near central stars of e.g. planetary nebulae or HII regions, are often observed. They are produced by fast winds from the stars which sweep out the nebular matter. V838 Mon has a B3V companion (Munari et al. 2002b). It is also plausible that V838 Mon itself was also of similar spectral type before the outburst (Tylenda, in preparation). According to the standard calibration (Drilling & Landolt 2000) B3V stars have  $\log L/L_\odot \simeq 3.5$  which, using the mean relation of Howarth & Prinja (1989), gives a mass loss rate of  $10^{-9} - 10^{-10} M_\odot/\text{yr}$ . Thus it is quite probable that the fast wind from the V838 Mon system has created the central hole in the dusty medium. The fact that the hole is strongly asymmetric implies that V838 Mon is moving relatively to the dusty medium. In the image taken on Sept. 2 the edge of the central hole in the east, south-east and south directions is sharp and very bright (compared to the emission behind the edge). Similar (although less evident) effect is also seen on other images (May 20, Oct. 28, Dec 17). Most probably we there see the regions compressed by the wind ahead of the moving star. On Oct. 28 nad Dec. 17 the same edge is less defined as there is a clear emission between the edge and the central star. This emission was absent on the images from May 20 and Sept. 2. Thus on Oct. 28 we have probably started seeing dust behind the central object. According to Eq. (2) this dust is  $\sim 0.1$  pc behind the star.

The above finding that V838 Mon is moving relatively to the dusty medium is difficult to understand if the medium were produced by mass loss from V838 Mon in the past. It is however quite natural if dust is of interstellar origin. We therefore conclude that dust illuminated by the light echo of V838 Mon is most probably of interstellar origin. This conclusion is also supported by the general

lack of spherical symmetries in the dust distribution, as discussed above. We do not confirm the assumption made in Bond et al. (2003) that the V838 Mon light echo has been produced by "a series of nested spherical dust shells centered on the star". Consequently their criticism of the merger scenario proposed by Soker & Tyllenda (2003) is not relevant. Note, however, that in view of the distance to V838 Mon being much larger than 1 kpc the scenario of Soker & Tyllenda should be revised (which will be done in a separate paper). Finally, as it is evident from the analysis and discussion made in the present paper, future observations of the V838 Mon light echo are of particular importance and interest.

*Acknowledgements.* The author is very grateful to Noam Soker for his comments on the initial version of this paper.

## References

- Bond, H. E., Henden, A., Levay, Z. G., et al. 2003, *Nature*, 422, 405
- Brown, N. J. 2002, *IAU Circ.*, 7785
- Chevalier, R. A. 1986, *ApJ*, 308, 225
- Couderc, P. 1939, *Ann. d'Astrophys.* 2, 271
- Drilling, J.S., Landoldt, A. U., 2000, in *Allen's Astrophysical Quantities*, the 4th edition, ed. A. N. Cox (Springer-Verlag New York) p. 381
- Henden, A., Munari, U., Schwartz, M. B. 2002 *IAU Circ.*, 7859
- Howarth, I. D., Prinja, R. K. 1989, *ApJS*, 69, 527
- Kimeswenger, S., Lederle, C., Schmeja, S., Armsdorfer, B. 2002, *MNRAS*, 336, L43
- Munari, U., Desidera, S., Henden, A. 2002b, *IAU Circ.*, 8005
- Munari, U., Henden, A., Kiyota, S., et al. 2002a, *A&A*, 389, L51
- Retter, A., Marom, A. 2003, *MNRAS*, submitted
- Soker, N., Tyllenda, R. 2003, *ApJ*, 582, L105
- Sparks, W. 1994, *ApJ*, 433, 19
- Wegner, W. 2000, *MNRAS*, 319, 771
- Xu, J., Crotts, A. P. S., Kunkel, W. E. 1995, *ApJ*, 451, 806